Inorg. Chem. **2004**, *43*, 4683–4692

Model of the Iron Hydrogenase Active Site Covalently Linked to a Ruthenium Photosensitizer: Synthesis and Photophysical Properties

Sascha Ott,[†] Magnus Borgström,[‡] Mikael Kritikos,[§] Reiner Lomoth,[‡] Jonas Bergquist,[||] Björn Åkermark,*[,†] Leif Hammarström,[‡] and Licheng Sun*[,†]

Departments of Organic Chemistry and Structural Chemistry, Arrhenius Laboratory, Stockholm University, S-10691 Stockholm, Sweden, Department of Physical Chemistry, BMC, Uppsala University, Box 579, S-75123 Uppsala, Sweden, and Department of Analytical Chemistry, BMC, Uppsala University, Box 599, S-75124 Uppsala, Sweden

Received December 15, 2003

A model of the iron hydrogenase active site with the structure [(μ-ADT)$Fe_2(CO)_6$] (ADT = azadithiolate (S–CH_2–NR–CH_2–S), (**2**: R = 4-bromophenyl, **3**: R = 4-iodophenyl)) has been assembled and covalently linked to a $[Ru(terpy)_2]^{2+}$ photosensitizer. This trinuclear complex **1** represents one synthetic step toward the realization of our concept of light-driven proton reduction. A rigid phenylacetylene tether has been incorporated as the linking unit in **1** in order to prolong the lifetime of the otherwise short-lived $[Ru(terpy)_2]^{2+}$ excited state. The success of this strategy is demonstrated by comparison of the photophysical properties of **1** and of two related ruthenium complexes bearing acetylenic terpyridine ligands, with those of $[Ru(terpy)_2]^{2+}$. IR and electrochemical studies reveal that the nitrogen heteroatom of the ADT bridge has a marked influence on the electronic properties of the [$Fe_2(CO)_6$] core. Using the Rehm–Weller equation, the driving force for an electron transfer from the photoexcited $*[Ru(terpy)_2]^{2+}$ to the diiron site in **1** was calculated to be uphill by 0.59 eV. During the construction of the trinuclear complex **1**, *n*-propylamine has been identified as a decarbonylation agent on the [(μ-ADT)$Fe_2(CO)_6$] portion of the supermolecule. Following this procedure, the first azadithiolate-bridged dinuclear iron complex coordinated by a phosphine ligand [(μ-ADT)$Fe_2(CO)_5PPh_3$] (**4**, R = 4-bromophenyl) was synthesized.

Introduction

Hydrogenases are a class of enzymes which catalyze the metabolism of hydrogen in cyanobacteria and other microorganisms. They can thereby function either as sinks for energy-rich electrons or provide the organisms with reducing power from hydrogen oxidation.[1−3] Hydrogenases are generally divided into two families, the nickel−iron (Ni−Fe) hydrogenases and the iron (Fe−Fe) hydrogenases, reflecting the different base metals present in the active site. Biologically, the two families differ from each other in that Ni−Fe hydrogenases seem to be more involved in hydrogen oxidation, whereas the iron hydrogenases tend to catalyze preferentially the production of hydrogen.[4,5] It is this remarkable ability of the iron hydrogenases which has inspired chemists of the bioinorganic community to synthesize close mimics of the active site of the natural system in the search for active hydrogen production catalysts.[6−8] From crystallographic as well as theoretical studies of the enzyme, the active site is known to consist of two iron nuclei, which are in bonding distance.[9,10] They are linked by a dithiolate bridge, recently suggested to possess the structure S−CH_2−NH−CH_2−S (azadithiolate = ADT).[11,12] Apart from a cysteine-linked

* Authors to whom correspondence should be addressed. E-mail: licheng.sun@organ.su.se (L.S.); bjorn.akermark@organ.su.se (B.A.).
[†] Department of Organic Chemistry, Stockholm University.
[‡] Department of Physical Chemistry, Uppsala University.
[§] Department of Structural Chemistry, Stockholm University.
[||] Department of Analytical Chemistry, Uppsala University.

(1) Nicolet, Y.; Lemon, B. J.; Fontecilla-Camps, J. C.; Peters, J. W. *Trends Biochem. Sci.* **2000**, *25*, 138−143.
(2) Peters, J. W. *Curr. Opin. Struct. Biol.* **1999**, *9*, 670−676.
(3) Frey, M. *ChemBioChem* **2002**, *3*, 152−160.
(4) Adams, M. W. W. *Biochim. Biophys. Acta* **1990**, *1020*, 115−145.
(5) Cammack, R. *Nature* **1999**, *397*, 214−215.
(6) Alper, J. *Science* **2003**, *299*, 1686−1687.
(7) Darensbourg, M. Y.; Lyon, E. J.; Smee, J. J. *Coord. Chem. Rev.* **2000**, *206−207*, 533−561.
(8) Evans, D. J.; Pickett, C. J. *Chem. Soc. Rev.* **2003**, *32*, 268−275.
(9) Peters, J. W.; Lanzilotta, W. N.; Lemon, B. J.; Seefeldt, L. C. *Science* **1998**, *282*, 1853−1858.
(10) Nicolet, Y.; Piras, C.; Legrand, P.; Hatchikian, E. C.; Fontecilla-Camps, J. C. *Structure* **1999**, *7*, 13−23.
(11) Nicolet, Y.; de Lacey, A. L.; Vernede, X.; Fernandez, V. M.; Hatchikian, E. C.; Fontecilla-Camps, J. C. *J. Am. Chem. Soc.* **2001**, *123*, 1596−1602.

10.1021/ic0303385 CCC: $27.50
Published on Web 07/02/2004

$[Fe_4S_4]$ cluster which is part of the electron-transfer chain to and from the active site, carbonyl and cyanide ligands occupy the remaining coordination sites around the iron nuclei.

The focus of the synthetic work has mainly been directed toward ligand exchange reactions on the "parent" dithiolate-bridged $[(\mu\text{-PDT})Fe_2(CO)_6]$ (PDT = propyldithiolate), a strategy benefiting in particular from the synthetic ease with which this complex is prepared.[13] The nature of introduced ligands ranges from isonitriles[14] and cyanides[15,16] to thioethers[17−19] and phosphines.[20] In this context, Darensbourg et al. have reported that $[(\mu\text{-H})(\mu\text{-PDT})Fe_2(CO)_4(PMe_3)_2]^+$ is a catalyst for H_2/D_2 scrambling,[20] whereas Rauchfuss et al. demonstrated that $[(\mu\text{-PDT})Fe_2(CO)_4PMe_3(CN)]^-$ serves as a catalyst for electrochemical hydrogen evolution.[21,22] We have recently described the concept of light-driven proton reduction, using a ruthenium−polypyridine complex as the light-harvesting component and a model of the iron hydrogenase as proton activation catalyst.[23]

Several potential problems have to be considered when pursuing such a concept. First, it is important that the lifetime of the sensitizer is sufficiently long to allow electron transfer to the diiron moiety. Second, it is conceivable that an attached iron unit could partly quench the excited state of the sensitizer by energy transfer. This would decrease the lifetime of the sensitizer and could seriously compete with electron transfer events. Third, of course, the redox potential of the excited state of the sensitizer should be sufficiently negative to permit electron transfer to the iron complex. In an exploratory study of ruthenium-sensitized hydrogen production, we chose $[Ru(terpy)_2]^{2+}$as the photosensitizer due to its geometric advantages over other Ru complexes with bidentate ligands.[24] We anticipated that the short lifetime of the excited state of this complex could be compensated at least partially by the introduction of an acetylene substituent, which concomitantly provides a synthetic handle for further elaboration to the trinuclear complex. Furthermore, this acetylenic bridge offers excellent control over the distance between the redox-active iron and ruthenium termini due to its linearity and rigidity. In contrast to the large amount of research which has been conducted on PDT-bridged diiron complexes, little work has been reported on the azadithiolate (ADT) analogues $[(\mu\text{-ADT})Fe_2(CO)_6]$[25−27] and the elucidation of their photophysical and electrochemical properties. This is particularly surprising since recent spectroscopic and theoretical studies have shown that this arrangement may play a crucial role in the natural system, providing a kinetically and thermodynamically favored pathway for hydrogen production.[11,12] We therefore decided to include this structural feature into our supramolecular assembly and **1** was selected as the target complex.

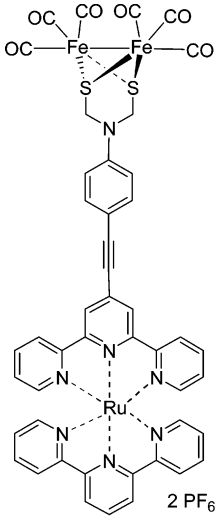

1

The construction of **1** coincided with an unexpected ligand substitution on the dinuclear iron site. *n*-Propylamine was identified as the agent responsible for the decarbonylation process. This new protocol could be utilized in the synthesis of the first phosphine-substituted ADT-bridged diiron complex **4**. The photophysical and electrochemical properties of the diiron complexes **2**−**6** were evaluated, and those of **1** were assessed in comparison with two novel reference complexes **8a**,**b**.

Results and Discussion

Synthesis. The trinuclear complex **1** was expected to become accessible by a Sonogashira cross coupling reaction[28] between an advanced diironhexacarbonyl precursor, featuring a suitable halogenated arene and 4′-ethynyl-2,2′:6′,2″-terpyridine. For this purpose, the bromo-equipped iron complex **2** and its iodo equivalent **3** were synthesized by applying a recently published procedure for the preparation of some related complexes.[25] Thus, the lithium salt of diironhexa-

(12) Fan, H.-J.; Hall, M. B. *J. Am. Chem. Soc.* **2001**, *123*, 3828−3829.
(13) Winter, A.; Zsolnai, L.; Huttner, G. *Z. Naturforsch.* **1982**, *37b*, 1430−1436.
(14) Lawrence, J. D.; Rauchfuss, T. B.; Wilson, S. R. *Inorg. Chem.* **2002**, *41*, 6193−6195.
(15) Lyon, E. J.; Georgakaki, I. P.; Reibenspies, J. H.; Darensbourg, M. Y. *Angew. Chem., Int. Ed.* **1999**, *38*, 3178−3180.
(16) Lyon, E. J.; Georgakaki, I. P.; Reibenspies, J. H.; Darensbourg, M. Y. *J. Am. Chem. Soc.* **2001**, *123*, 3268−3278.
(17) Razavet, M.; Davies, S. C.; Hughes, D. L.; Pickett, C. J. *Chem. Commun.* **2001**, 847−848.
(18) Razavet, M.; Borg, S. J.; George, S. J.; Best, S. P.; Fairhurst, S. A.; Pickett, C. J. *Chem. Commun.* **2002**, 700−701.
(19) George, S. J.; Cui, Z.; Razavet, M.; Pickett, C. J. *Chem. Eur. J.* **2002**, *8*, 4037−4046.
(20) Zhao, X.; Georgakaki, I. P.; Miller, M. L.; Mejia-Rodriguez, R.; Chiang, C.-Y.; Darensbourg, M. Y. *Inorg. Chem.* **2002**, *41*, 3917−3928.
(21) Gloaguen, F.; Lawrence, J. D.; Rauchfuss, T. B. *J. Am. Chem. Soc.* **2001**, *123*, 9476−9477.
(22) Gloaguen, F.; Lawrence, J. D.; Rauchfuss, T. B.; Benard, M.; Rohmer, M.-M. *Inorg. Chem.* **2002**, *41*, 6573−6582.
(23) Ott, S.; Kritikos, M.; Åkermark, B.; Sun, L. *Angew. Chem., Int. Ed.* **2003**, 3285−3288.
(24) Hammarström, L.; Barigelletti, F.; Flamigni, L.; Indelli, M. T.; Armaroli, N.; Calogero, G.; Guardigli, M.; Sour, A.; Collin, J.-P.; Sauvage, J.-P. *J. Phys. Chem. A* **1997**, *101*, 9061−9069.
(25) Lawrence, J. D.; Li, H.; Rauchfuss, T. B. *Chem. Commun.* **2001**, 1482−1483.
(26) Lawrence, J. D.; Li, H.; Rauchfuss, T. B.; Benard, M.; Rohmer, M.-M. *Angew. Chem., Int. Ed.* **2001**, *40*, 1768−1771.
(27) Li, H.; Rauchfuss, T. B. *J. Am. Chem. Soc.* **2002**, *124*, 726−727.
(28) Sonogashira, K.; Tohda, Y.; Hagihara, N. *Tetrahedron Lett.* **1975**, 4467−4470.

Scheme 1

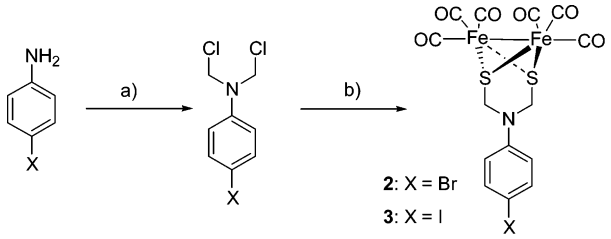

[a] (1) *p*-CH_2O, CH_2Cl_2, 3 h, (2) $SOCl_2$. [b] $[(Li-S)_2Fe_2(CO)_6]$, THF, − 78 °C, 10 min, 76% for **2**, 76% for **3**.

carbonyl disulfide[29] was reacted with the respective *N*,*N*-bis(chloromethyl)-4-haloaniline, which in turn was synthesized from the *p*-haloaniline in two steps (Scheme 1).

Initial acetylene coupling experiments were conducted with the bromo-substituted compound **2**. However, stirring this complex in the presence of trimethylsilyl acetylene, catalytic amounts of copper iodide and $[(PPh_3)_2PdCl_2]$ (ca. 5 mol %) in a mixture of toluene and *n*-propylamine at elevated temperature did not afford the phenylacetylene **5**. Instead, a side-product was isolated in a yield of ca. 10%, in addition to the recovered starting material. Whereas the low reactivity of electron-rich bromoarene **2** in Sonogashira cross coupling reactions may not be surprising,[30] IR-studies of the product revealed that the coordination sphere around the dimeric iron site had been altered. A pattern typical for a monosubstituted complex of type $[Fe_2(CO)_5X]$ was observed in the carbonyl region of the IR spectrum.[31] Furthermore, the ^1H NMR signal for the methylene protons in the bridge, which appears as a singlet in the starting material, had split into two doublets ($J = 12.2$ Hz), consistent with a decreased symmetry of the system. The nature of the introduced ligand could unambiguously be identified by single-crystal X-ray diffraction analysis (Figure 4). It revealed that a triphenylphosphine ligand from the palladium catalyst had entered the coordination sphere of the dimeric iron site, thereby replacing one CO ligand.

In an attempt to elucidate the role of the amine in this ligand substitution, **2** and an excess of triphenylphosphine were stirred in *n*-propylamine and in triethylamine in two separate experiments. Whereas the reaction in the primary amine resulted in quantitative ligand exchange after a few hours, no such substitution could be detected in the tertiary amine after 24 h (Scheme 2). From this experiment it appears that the nucleophilic *n*-propylamine is responsible for a decrease of the iron carbonyl bond stability and thereby facilitates the carbonyl-to-phosphine ligand exchange. Whether the initial attack proceeds on the iron center or on the carbonyl ligand has not been determined in this study. Ligand exchange reactions, facilitated by nucleophiles such as halides or amines, are not unprecedented and have been reported for Fe^0 carbonyl species and other transition-metal carbonyl clusters.[32,33] Noteworthy is the fact that the mono-

Scheme 2: Carbonyl-Triphenylphosphine Ligand Exchange Promoted by (*n*-Pr)NH_2

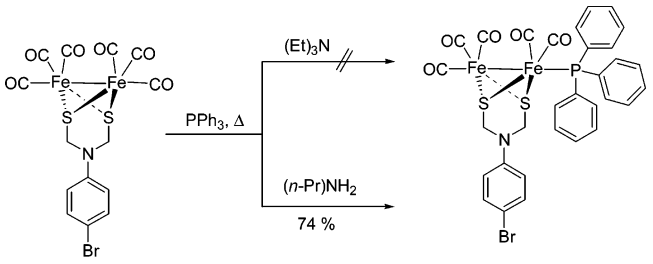

substituted complex **4** is obtained exclusively, even at prolonged reaction times and in the presence of a large excess of triphenylphosphine. Two factors could account for this phenomenon. The steric demand of the bulky triphenylphosphine ligand cannot be satisfied on both iron centers due to the presence of the aryl group which resides directly over one CO ligand. Furthermore, the increased electron density at the substituted iron may be communicated to the adjacent iron center, resulting in a decreased electrophilicity of the monosubstituted complex.

To avoid ligand substitution, a tertiary amine was used in the palladium-mediated cross coupling reaction for the construction of the arylacetylene bond present in **1**. Most gratifyingly, we found that iodoarene **3**, which is more reactive than the bromo-correspondent **2**, couples smoothly to trimethylsilyl acetylene under these modified conditions (Scheme 3). The acetylenic diiron complex **5** was isolated in excellent yield and was characterized by standard techniques, including X-ray analysis (Figure 3).

Subjecting 4′-ethynyl-2,2′:6′,2″-terpyridine[34,35] instead of trimethylsilyl acetylene to otherwise identical coupling conditions resulted in the formation of the terpyridine-equipped diiron complex **6**. Solutions of **6** in organic solvents are unstable at room temperature and decompose within minutes upon exposure to light, presumably due to light-induced decarbonylation followed by intermolecular terpyridine complexation. However, as a freshly prepared solution in methanol which is kept in the dark, ligand **6** coordinates readily to the (terpy)Ru fragment,[36] giving rise to the desired trinuclear complex **1** (Scheme 3).[23]

Over the past few years, the utilization of acetylene moieties has become a popular strategy to prolong the lifetime of the otherwise short-lived $[Ru(terpy)_2]^{2+}$ ($\tau < 1$ ns) excited state. For example, ethynylterpyridine substitution on one terpyridine ligand results in an increase of the excited-state lifetime to 55 ns,[37] whereas the introduction of an ethynylpyrene prolongs the lifetime to 560 ns, although as a mixture of metal- and pyrene-centered triplet excited states

(29) Brandt, P. F.; Lesch, D. A.; Stafford, P. R.; Rauchfuss, T. B. *Inorg. Synth.* **1997**, *31*, 112−116.
(30) Singh, R.; Just, G. *J. Org. Chem.* **1989**, *54*, 4453−4457.
(31) Ellgen, P. C.; Gerlach, J. N. *Inorg. Chem.* **1973**, *12*, 2526−2532.
(32) Angelici, R. J. *Acc. Chem. Res.* **1972**, *5*, 335−342.
(33) Lavigne, G. *The Chemistry of Metal Cluster Complexes*; Shriver, D. F., Kaesz, H. D., Adams, R. D., Eds.; VCH: New York, 1990.
(34) Potts, K. T.; Konwar, D. *J. Org. Chem.* **1991**, *56*, 4815−4816.
(35) Grosshenny, V.; Romero, F. M.; Ziessel, R. *J. Org. Chem.* **1997**, *62*, 1491−1500.
(36) Norrby, T.; Börje, A.; Åkermark, B.; Hammarström, L.; Alsins, J.; Lashgari, K.; Norrestam, R.; Mårtensson, J.; Stenhagen, G. *Inorg. Chem.* **1997**, *36*, 5850−5858.
(37) Benniston, A. C.; Grosshenny, V.; Harriman, A.; Ziessel, R. *Angew. Chem., Int. Ed. Engl.* **1994**, *33*, 1884−1885.

Scheme 3

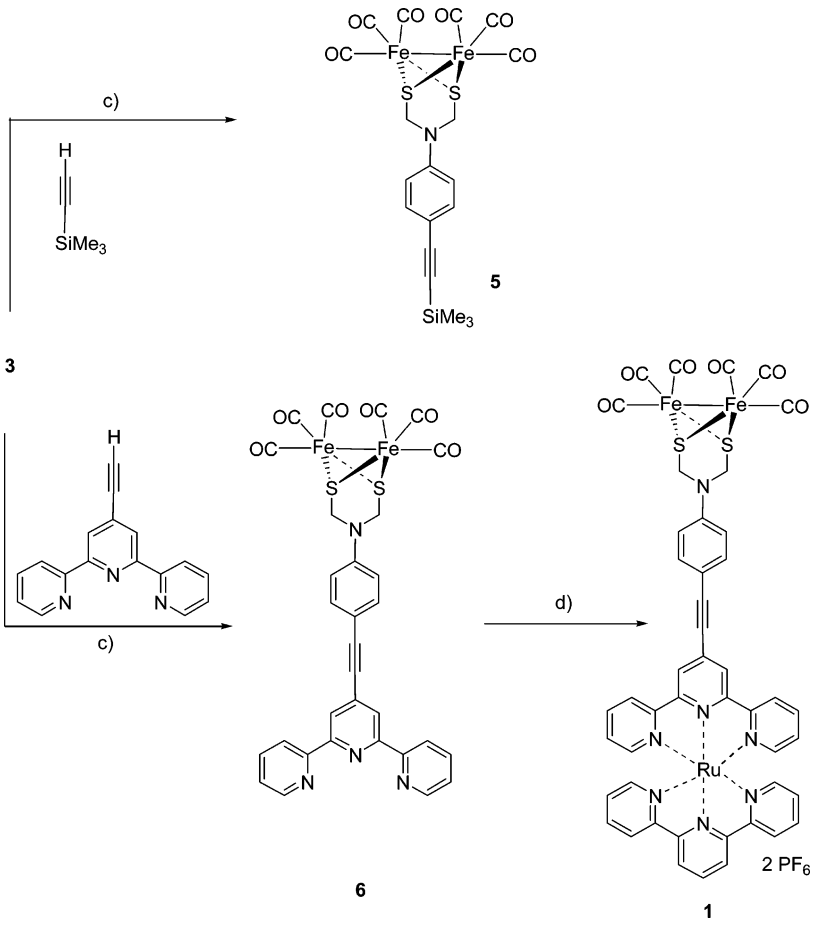

[c] [$(PPh_3)_2PdCl_2$], CuI, Et_3N, toluene, 40 °C, 3 h, 91% for **5**, 57% for **6**. [d] [(Terpy)$RuCl_2$(DMSO)], MeOH, reflux, 4 h, 29%.

in a quasi equilibrium.[38] Despite this extensive utilization of acetylene substituents, we were surprised to find that no work has been reported on the most basic phenylethynyl-substituted $[Ru(terpy)_2]^{2+}$. To have a reference system comparable to **1**, the 4-(*N*-piperidyl)phenylethynyl-terminated $[Ru(terpy)_2]^{2+}$ complex **8a** as well as its phenylethynyl-analogue **8b** were synthesized in procedures analogous to that for the preparation of **1**. Hence, iodo-4-(*N*-piperidyl)-benzene[39] was reacted with 4′-ethynyl-2,2′:6′,2″-terpyridine[35] to produce the acetylenic ligand **7a** and phenyl acetylene was reacted with 4′-[((trifluoromethyl)sulfonyl)oxy]-2,2′:6′,2″-terpyridine[34,40] to form **7b**. Subsequently, both ligands were separately coordinated to the (terpy)Ru fragment in refluxing ethanol, thereby forming **8a** and **8b** (Scheme 4).

Scheme 4

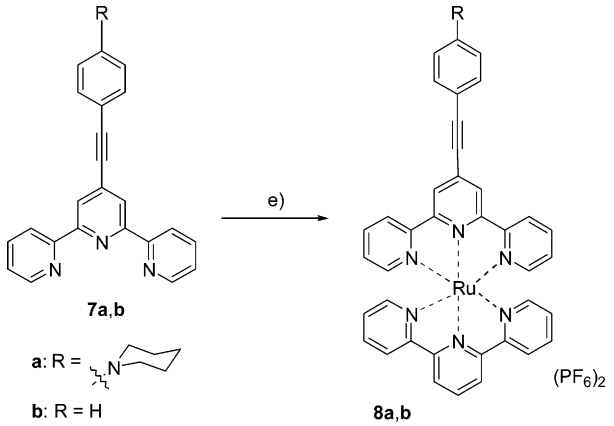

[e] [(Terpy)$RuCl_2$(DMSO)], EtOH, reflux, 16 h, 53% for **8a**, 64% for **8b**.

IR Spectroscopy. The IR spectra of complexes **1**−**3**, **5**, and **6** (in solution of CH_2Cl_2) are literally identical in the CO region and feature three signals at 2076, 2038, and 2001 cm^{-1}. This result clearly indicates that there is only a negligible electronic communication between the redox active ruthenium and iron termini in the ground state. It might therefore not be surprising that these values also correlate with those reported for other azadithiolate-bridged diiron complexes.[26,27] It seems, however, that the nitrogen heteroatom in the ADT bridge slightly influences the electronic properties of the carbonyl ligands. Compared to the IR spectrum of [(μ-PDT)$Fe_2(CO)_6$] (ν_{CO} = 2073, 2034, 1998 in CH_2Cl_2), the CO frequencies are shifted by 3−4 cm^{-1} toward higher wavenumbers. Reflecting the changed coordination sphere around the iron cations, the IR spectrum of the triphenylphosphine-substituted complex **4** exhibits markedly different resonances in the carbonyl region at 2048,

(38) Harriman, A.; Hissler, M.; Khatyr, A.; Ziessel, R. *Chem. Commun.* **1999**.
(39) Effenberger, F.; Agster, W.; Fischer, P.; Jogun, K. H.; Stezowski, J. J.; Daltrozzo, E.; Kollmannsberger-von Nell, G. *J. Org. Chem.* **1983**, *48*, 4649−4658.
(40) Constable, E. C.; Ward, M. D. *J. Chem. Soc., Dalton Trans.* **1990**, 1405−1409.

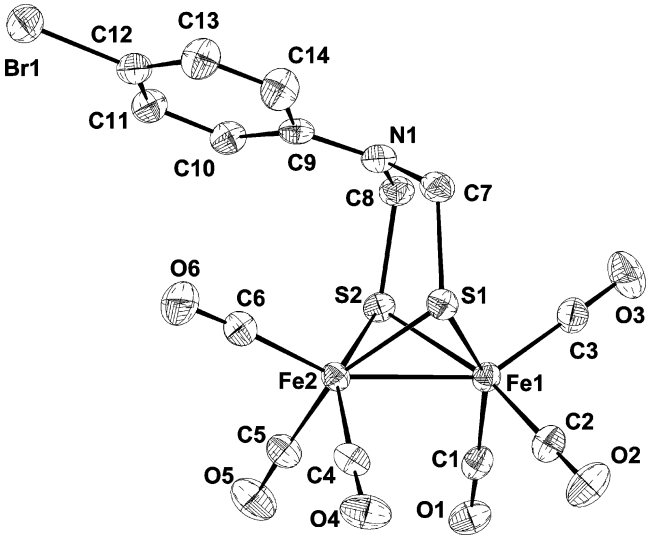

Figure 1. ORTEP (ellipsoids at 30% probability level) view of $C_{14}H_8BrNO_6S_2Fe_2$ (**2**).

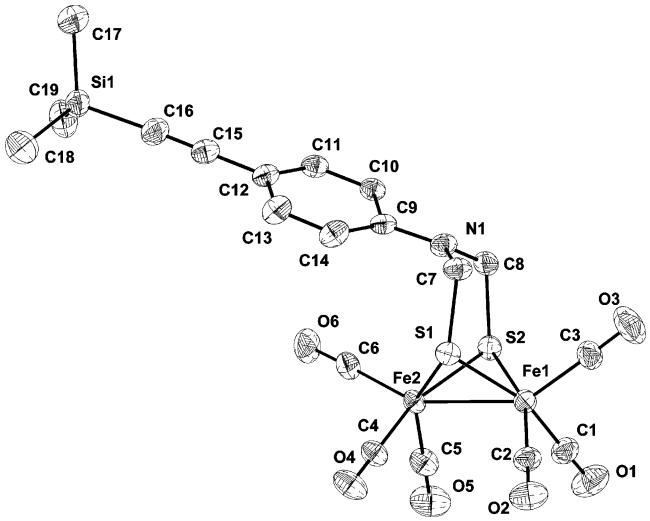

Figure 2. ORTEP (ellipsoids at 30% probability level) view of $C_{19}H_{17}SiNO_6S_2Fe_2$ (**5**).

1990, and 1935 cm^{-1}. Analogous to the situation in the all-carbonyl complexes, these values are shifted slightly toward higher energy compared to those found for the PDT-bridged $[(\mu\text{-PDT})Fe_2(CO)_5(PPh_3)]$ analogue.[41] These slight differences indicate that the nitrogen in the bridge has a small impact on the carbonyl ligands.

Solid-State Structures. Solid-State Structure of 2 and 5. The $[(\mu\text{-S})_2Fe_2(CO)_6]$ units of **2** and **5** are very similar (Figures 1 and 2) and are to a large extent analogous to those found in other $[(\mu\text{-S})_2Fe_2(CO)_6]$ structures reported.[26] In the central $[(\mu\text{-SR})_2Fe_2(CO)_6]$ unit the two Fe atoms and the two S atoms form a butterfly conformation in which the metal atoms are connected to each other through an Fe−Fe single bond (2.494(1) and 2.5035(8) Å for **2** and **5**, respectively). In contrast to the Fe−Fe distances the S···S contacts vary slightly more, 3.075(2) Å in **2** and 3.058(2) Å in **5**. In both complexes the two $Fe(CO)_3$ units are nearly eclipsed. The

(41) Hasan, M. M.; Hursthouse, M. B.; Kabir, S. E.; Malik, K. M. A. *Polyhedron* **2001**, *20*, 97−101.

Table 1: Selected Bond Lengths (Å) for **2**, **4**, and **5**

	2	4	5
Fe1−Fe2	2.494(1)	2.5094(9)	2.5035(8)
Fe1−S1	2.265(2)	2.2860(12)	2.2569(10)
Fe1−S2	2.270(2)	2.2705(13)	2.2603(11)
Fe2−S1	2.263(2)	2.2533(12)	2.2660(10)
Fe2−S2	2.283(2)	2.2669(14)	2.2516(11)
Fe1−C1	1.815(7)	2.2803(13)	1.800(5)
Fe1−C2	1.816(7)	1.761(5)	1.796(5)
Fe1−C3	1.789(7)	1.765(5)	1.796(5)
Fe2−C4	1.802(7)	1.779(5)	1.797(5)
Fe2−C5	1.803(7)	1.806(5)	1.793(4)
Fe2−C6	1.804(7)	1.775(5)	1.796(5)
S1−C7	1.865(6)	1.864(5)	1.850(4)
S2−C8	1.858(6)	1.858(5)	1.864(4)
Br1−C11/12	1.892(6)	1.892(6)	na
N1−C7			1.428(5)
N1−C8			1.424(5)
N1−C9			1.407(4)
C12−C15	na	na	1.432(6)
C15−C16	na	na	1.198(7)
Si1−C16	na	na	1.824(5)

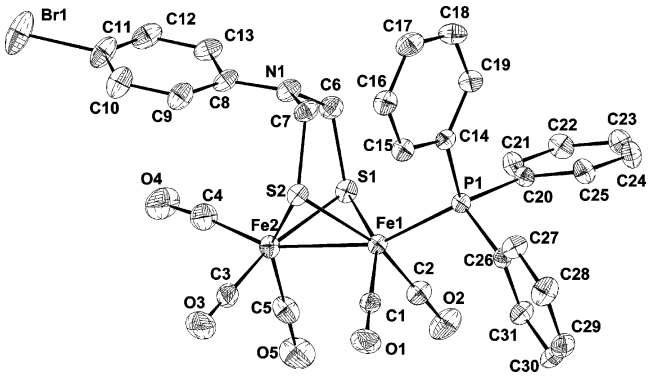

Figure 3. ORTEP (ellipsoids at 30% probability level) view of $C_{31}H_{24}BrNO_5PS_2Fe_2$ (**4**).

Fe−C and C−O distances and Fe−C−O angles are all normal with one exception. The Fe−C−O angles for the carbonyls closest to the amine functionality (i.e. trans to the Fe−Fe bond) in **2** and **5** deviate significantly from the expected 180° linear arrangements with values of 175.6(7)° and 174.2(6)°, respectively. The nonbonding C···N distance between the amine and the closest carbonyl carbon atom in **2** (3.578(8) Å) is longer than the equivalent distance in **5** (3.506(5) Å). Moreover, the nitrogen atom deviates from the plane defined by C7, C8, and C9 by 0.174(5) Å in **2** and by 0.147(3) Å in **5**. This nonplanarity ruptures the potential π-conjugation between the phenyl ring and the nitrogen p-orbital. In **5**, the acetylenic C−C triple bond and the Si−C single bonds in the trimethylsilyl group adopt expected values. Selected bond distances are summarized in Table 1.

Solid-State Structure of 4. The molecular structure of **4** is illustrated in Figure 4. In **4**, the CO group located trans to the Fe−Fe bond has been replaced by the PPh_3 ligand. This positioning of the phosphine group is consistent with its bulkiness. The Fe−P bond distance (2.253(1) Å) is identical to that reported for the related toluenedithiolate $[(\mu_2\text{-}SC_7H_6S)Fe_2(CO)_5(PPh_3)]$.[41] In **4**, the Fe−Fe single bond is somewhat elongated (2.5094 (9) Å) compared to those in **2** and **5**. As found for **2** and **5**, the CO group closest to the amine functionality is significantly bent, 173.6(6)°. The carbonyl to amine (i.e. C4···N1) nonbonding distance is 3.518(7) Å.

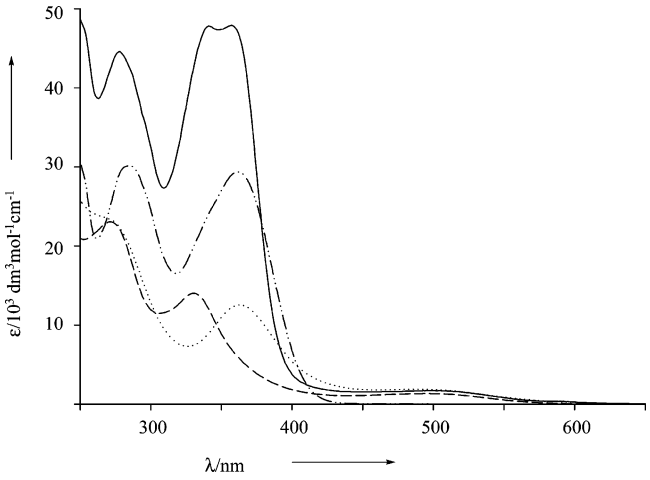

Figure 4. Electronic absorption spectra of **2** (— —), **4** (·····), **6** (—), and **7a** (—·····—) recorded in CH_2Cl_2.

Table 2: Electrochemical Data for Complexes **1**−**5** and **8a,b**[a]

compound	$E_{red/ox}$ ($Ru^{II/III}$)	E_{pa}	E_{pc} (Fe_2-site)	E_{pc} (terpy)
2	na	0.54[b]	−1.53[b]	na
3	na	0.56[b]	−1.54[b]	na
4[c]	na	0.34[i]	−1.90[i]	na
5	na	0.64[i]	−1.56[i]	na
1	0.91	0.65[i]	−1.49[i]	−1.67;[d] −1.89[d]
8a	0.95	0.50[i]	na	−1.60; −1.89
8b	0.91	na	na	−1.57; −1.89

[a] All potentials were recorded for deaerated, 1 mM solutions in acetonitrile containing Bu_4NPF_6 (0.1 M) as supporting electrolyte and are given vs $Fc^{+/0}$; scan rate 50 mV/s. Given are anodic (E_{pa}) and cathodic peak potentials E_{pc}. [b] Irreversible. [c] Measured in CH_2Cl_2. [d] Detected by differential pulse voltammetry.

Further, the N1 atom is displaced 0.196(4) Å from the plane defined by C6, C7, and C8. These metrical data show that the geometry of the azadithiolate functionality is rather insensitive toward ligand substitution on the Fe atoms.

Electrochemistry. To assess a potential driving force for an electron transfer from the photoexcited $[Ru(terpy)_2]^{2+}$ portion to the diiron site in **1**, cyclic voltammograms were recorded for all diiron and ruthenium complexes reported herein (Table 2 and Supporting Information). This is of particular interest since no electrochemical data of azadithiolate-bridged diiron complexes have been reported in the literature to date. An irreversible oxidation of the iron complexes **1**−**3** and **5** is observed at a potential around 0.60 ± 0.05 V vs $Fc^{+/0}$. Reflecting the donor capacity of the triphenylphosphine ligand, complex **4** exhibits an irreversible oxidation at a potential which is lower by 0.25 V compared to those of the all-carbonyl analogues. A similar trend has been observed by Poilblanc et al. during the introduction of tertiary phosphines on $[Fe_2(\mu\text{-}SR)_2(CO)_6]$-type of complexes.[42] An interesting point, however, arises from an inspection of the cyclic voltammogram of the piperidine-containing $[Ru(terpy)_2]^{2+}$ complex **8a**, which exhibits an irreversible oxidation at 0.50 V. This oxidation, which undoubtedly is centered on the tertiary aniline portion, is suspiciously similar to that observed for complexes **1**−**3** and **5** suggesting that the oxidation of the diiron complexes may be located on the tertiary aniline portion. Efforts to determine the exact location of the electron hole in oxidized **2**, **3**, and **5** by spectroscopic techniques (ESR, UV/vis) were unsuccessful due to the instability of the oxidized species. On the cathodic scan, the all-carbonyl iron complexes **2**, **3**, and **5** typically feature an irreversible reduction around −1.55 ± 0.02 V, whereas the electron-enriched complex **4** is reduced at more negative potential at −1.90 V (recorded in CH_2Cl_2). In comparison with $[(\mu\text{-PDT})Fe_2(CO)_6]$ which is reduced at −1.67 V vs $Fc^{+/0}$,[43] the azadithiolate bridge seems to have a considerable influence on the reduction potentials, rendering the ADT-bridged complexes **2**, **3**, and **5** more susceptible for reduction by more than 100 mV. This feature makes $[(\mu\text{-ADT})Fe_2(CO)_6]$ complexes superior acceptors in electron-transfer processes over the all-carbon bridged analogues.

The Ru(II)/Ru(III) couple in the $[Ru(terpy)_2]^{2+}$ complexes **1**, **8a**, and **8b** is observed at 0.93 ± 0.02 V. Reduction of **1** at −1.49 V proceeds at a potential slightly less negative than those usually observed for the reduction of the terpyridine ligands and can thus be assigned to the reduction of the diiron portion. The remaining reduction waves for **1** at −1.67 V and −1.89 V and around −1.6 and −1.89 V for **8a** and **8b** are typical for $[Ru(terpy)_2]^{2+}$ complexes and arise from the reduction of the terpyridine ligands. The driving force for an electron transfer from the photoexcited $*[Ru(terpy)_2]^{2+}$ to the diiron site in **1** can be calculated from these electrochemical potentials in conjunction with the excited-state energy (see emission section).

Electronic Absorption Spectra. The UV/Vis spectra of the dinuclear iron complexes **2**−**4** are dominated by a strong absorption in the UV region around 270 nm. A second intense absorption is visible in the near UV and shifts substantially depending on the coordination sphere around the iron nuclei. For example, it can be detected around 330 nm for **2** and **3** (graph not shown) up to 363 nm in **4** (Figure 5). This might be an indication for the involvement of metal as well as ligand orbitals in this transition. A broad and featureless absorption reaching up to 600 nm with an extinction coefficient of maximal 1800 M^{-1} cm^{-1} is responsible for the dark red color of these iron coordination compounds. The piperidine-containing terpyridine **7a** features a strong absorption at 362 nm in addition to a band in the far UV. The UV/Vis spectrum of ligand **6** exhibits three intense absorptions at 278, 341, and 357 nm, thereby suggesting that it can be regarded as a linear combination of the spectra of **2** and that of the reference ligand **7a** (Figure 4).

The trinuclear ruthenium−diiron complex **1** and the reference complexes **8a** and **8b** display electronic absorption spectra typical for $[Ru(terpy)_2]^{2+}$ type of complexes (Figure

(42) Mathieu, R.; Poilblanc, R.; Lemoine, P.; Gross, M. *J. Organomet. Chem.* **1979**, *165*, 243−252.

(43) The discrepancy of this value to the one reported in Razavet, M.; Davies, S. C.; Hughes, D. L.; Barclay, J. E.; Evans, D. J.; Fairhurst, S. A.; Liu, X.; Pickett, C. J. *J. Chem. Soc., Dalton Trans.* **2003**, 586−595 is a result of different reference systems. All potentials reported herein are vs $Fc^{+/0}$.

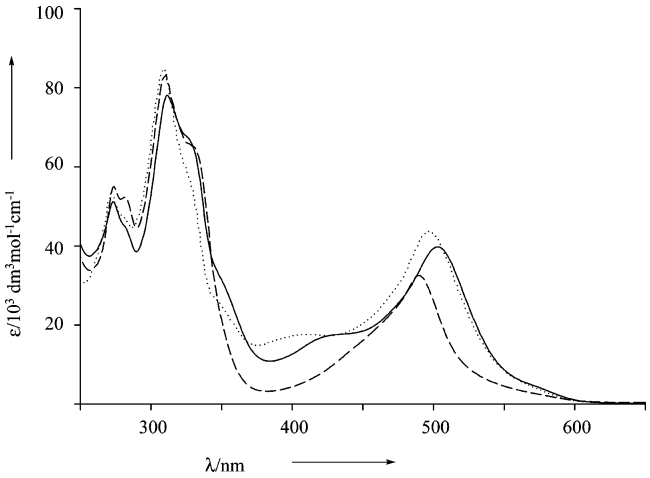

Figure 5. Electronic absorption spectra of **1** (—), **8a** (·····), and **8b** (— —), recorded in CH_2Cl_2.

5).[44] The strongest absorption in the UV around 310 nm is usually attributed to terpyridine-centered $\pi \rightarrow \pi^*$ transitions. The longest wavelength absorption around 500 nm is caused by metal-to-ligand charge-transfer transitions of the ruthenium moiety. The band arising from this transition seems to overlay the weak absorption from the diiron portion in **1**.

Emission Data. The excited-state energy of complexes **1** and **8a**,**b** were determined from the emission spectra recorded in a solvent glass at 77 K (not shown). The peak with the highest energy in the vibrational progression has been shown to give a good estimate for the exited state energy.[24,45,46] For complexes **1**, **8a**, and **8b** the excited-state energies were calculated to be 1.89, 1.89, and 1.91 eV, respectively. As an effect of the better electron accepting capacity of the ligands in these complexes, these values are slightly lower than that for $[Ru(terpy)_2]^{2+}$ (2.07 eV).[47] The driving force for electron transfer from the ruthenium to the diiron site could be calculated with the Rehm−Weller equation.[48] Using the reduction potentials from the cyclic voltammetry data and omitting the work term arising from Coulombic interactions the driving force was calculated to be uphill with $\Delta G^\circ = 0.59$ eV.[49] The luminescence properties are summarized in Table 3.

The acetylene linkage in **1** was incorporated to satisfy two different requirements: to gain precise control over the spatial separation between the redox active iron and ruthenium termini and, more importantly, to increase the lifetime of the $[Ru(terpy)_2]^{2+}$ photosensitizer. The success of this strategy was determined by comparison of the excited-state properties of **1** and two reference complexes, the 4-(*N*-piperidyl)phenylethynyl- **8a** and the phenylethynyl-substituted $[Ru(terpy)_2]^{2+}$ **8b**, with those of unsubstituted $[Ru(terpy)_2]^{2+}$.

Table 3: Luminescence Properties of Complexes **1**, **8a**, and **8b** and $[Ru(terpy)_2]^{2+}$ [51]

complex	295 K λ_{ems}/nm	ϕ_{ems}	τ_{ems}/ns	77 K λ_{ems}/nm
1	674	2×10^{-5}	6.5	657
8a	675	1.5×10^{-4}	23	658
8b	666	1.5×10^{-4}	13.5	650
$[Ru(terpy)_2]^{2+}$		$<10^{-5}$	0.250	598

The excited-state decay, as determined from the time-resolved emission decay traces, gave lifetimes of 23 ns for **8a**, 13.5 ns for **8b**, and 6.5 ns for **1** (see Supporting Information). A smaller lifetime component (c.a. 15% of the total amplitude) with $\tau \approx 2$ ns was present in the samples of all three complexes, and is attributed to a decomposition product.[50] Flash photolysis transient absorption experiments with ca. 10 ns resolution show excited-state decays in agreement with the emission data.

First, we note that the excited-state lifetimes in **1** and **8a**,**b** are much longer than that in the parent, unsubstituted $[Ru(terpy)_2]^{2+}$ ($\tau = 250$ ps).[51] This substantial improvement can be explained by a delocalization of the MLCT excited state over the conjugated phenylacethylene substituent. This may decrease the rate of population of metal-centered states that lead to rapid decay to the ground state, in analogy with the results of previous studies.[24,37,45,46]

Second, the excited-state decay is significantly faster in **1** than in **8a** and **8b**. The quenching rate constant k_q can be estimated as $k_q = 1/\tau_{\mathbf{1}} - 1/\tau_{\mathbf{8a}} = 1.1 \times 10^8\ s^{-1}$. Since the electron transfer to the diiron moiety is strongly endothermic, the quenching is not induced by electron transfer but rather by dipole−dipole energy transfer. A calculation of the rate constant using Förster's equation[52] with the orientation factor κ set to 1 and a donor−acceptor distance of 8.5 Å gave a value of a similar magnitude as the experimental one. The exact location of the excited state in **1** is somewhat ambiguous but a donor−acceptor distance of 8.5 Å is not unreasonable, making Förster energy transfer a plausible explanation for the observed quenching in **1**. Energy transfer quenching with a rate constant of $1.1 \times 10^8\ s^{-1}$ is modest and will probably not seriously compete with electron transfer in the next generation of $Ru-Fe_2$ complexes.

Conclusion

We have synthesized a model of the iron hydrogenase active site $[(\mu\text{-ADT})Fe_2(CO)_6]$ and have covalently linked

(44) Sauvage, J.-P.; Collin, J.-P.; Chambron, J.-C.; Guillerez, S.; Coudret, C.; Balzani, V.; Barigelletti, F.; De Cola, L.; Flamigni, L. *Chem. Rev.* **1994**, *94*, 993−1019.
(45) Caspar, J. V.; Meyer, T. J. *Inorg. Chem.* **1983**, *22*, 2444−2453.
(46) Treadway, J.; Loeb, B.; Lopez, R.; Anderson, P. A.; Keene, F. R.; Meyer, T. J. *Inorg. Chem.* **1996**, *35*, 2242−2246.
(47) Maestri, M.; Armaroli, N.; Balzani, V.; Constable, E. C.; Cargill Thompson, A. M. W. *Inorg. Chem.* **1995**, *34*, 2759−2767.
(48) Rehm, D.; Weller, A. *Isr. J. Chem.* **1970**, *8*, 259−271.
(49) The driving force for a second electron transfer from a regenerated and photoexcited $[Ru(terpy)_2]^{2+}$ to an already reduced diiron complex will be even more endothermic. However, protonation of the monoreduced diiron site might compensate for this effect.
(50) The amplitude of the 2 ns component had increased to 50−75% of the total amplitude when the experiments were repeated several months later, with solutions freshly prepared from the powder sample that had been stored in the freezer. This strongly suggests that the 2 ns component is a decomposition product formed in the powder. Possibly, the triple bond is oxidized by O_2, which gives a complex with a lifetime closer to that for the parent $[Ru(terpy)_2]^{2+}$. In addition, a minor component (1−5% of the amplitude) with a lifetime of 150 ns was present in all the samples, probably from an impurity.
(51) Winkler, J. R.; Netzel, T. L.; Creutz, C.; Sutin, N. *J. Am. Chem. Soc.* **1987**, *109*, 2381−2392.
(52) Förster, T. *Discuss. Faraday Soc.* **1959**, 7−17.

Table 4. Selected Crystal Data for $C_{14}H_8BrNO_6Fe_2$ (**2**), $C_{31}H_{24}BrNO_5PS_2Fe_2$ (**4**), and $C_{19}H_{17}SiNO_6S_2Fe_2$ (**5**)

	2	**4**	**5**
empirical formula	$C_{14}H_8BrNO_6S_2Fe_2$	$C_{31}H_{24}BrNO_5PS_2Fe_2$	$C_{19}H_{17}SiNO_6S_2Fe_2$
fw	541.94	777.23	559.25
cryst syst	triclinic	triclinic	triclinic
space group	P-1 (No. 2)	P-1 (No. 2)	P-1 (No. 2)
a, Å	7.816(2)	9.4590(17)	7.6647(12)
b, Å	11.046(3)	10.1888(19)	9.6722(15)
c, Å	11.353(3)	17.330(3)	16.918(3)
α, °	74.81(3)	73.47(2)	76.96(2)
β, °	86.93(3)	78.93(2)	81.12(2)
γ, °	80.04(3)	88.07(2)	89.96(2)
V, Å^3	931.6(4)	1571.0(5)	1206.5(4)
Z	2	2	2
ρ_{calc}, g cm^{-3}	1.932(1)	1.643(1)	1.539(1)
temperature, K	293	293	293
μ (MoKα), (mm^{-1})	3.955	2.420	1.458
N(obs) ($I > 2\sigma(I)$)/*N*(par)	2152/236	4467/388	3425/283
goodness of fit	0.915	1.15	1.25
R1,[a] wR2, ($I > 2\sigma(I)$)	0.0384, 0.0813	0.0522, 0.1365	0.0337, 0.0822
$\Delta\rho_{max}$, $\Delta\rho_{min}$ (e/Å^3)	0.69, −0.68	1.05, −1.73	0.86, −1.27

[a] *R* values are defined as $R1 = \sum||F_o|-|F_c||/\sum|F_o|$, $wR2 = [\sum[w(F_o^2-F_c^2)^2]/\sum[w(F_o^2)^2]]^{1/2}$.

it to a $[Ru(terpy)_2]^{2+}$ photosensitizer in a first attempt to afford proton reduction by light. During the synthesis of **1**, *n*-propylamine has been identified as a decarbonylation agent at the hexacarbonyldiiron core, and the new protocol has been applied for the synthesis of a diiron complex **4** coordinated by a phosphine ligand. The IR spectra of all novel $[(\mu\text{-ADT})Fe_2(CO)_6]$ complexes were literally identical in the CO region, pointing toward an electronic insulation of the iron and ruthenium termini in the ground state. In comparison with the IR spectrum of $[(\mu\text{-PDT})Fe_2(CO)_6]$, the redox-active nitrogen of the ADT bridge in **1**−**3**, **5**, and **6** seems to have a small impact on the CO frequencies. Furthermore, the nitrogen heteroatom in the $[(\mu\text{-ADT})Fe_2(CO)_6]$ complexes **1**−**3** and **5** has a marked effect on their respective reduction potentials. The former complexes are reduced at a potential more than 100 mV less negative than the all-carbon bridged $[(\mu\text{-PDT})Fe_2(CO)_6]$. This finding renders the ADT-bridged complexes superior to their PDT analogues as acceptors in electron-transfer processes.

Compared to the unsubstituted $[Ru(terpy)_2]^{2+}$ which exhibits an excited-state lifetime of 250 ps,[51] introduction of an acetylene tether resulted in increased lifetimes in **1**, **8a**, and **8b**. In **1** the observed excited-state lifetime was 6.5 ns, substantially shorter than in **8a** (23 ns) and **8b** (13.5 ns). Presumably, dipole−dipole energy transfer with a rate of 1.1×10^8 s^{-1} is responsible for the decrease of the excited-state lifetime in **1**. From the excited-state energy and the electrochemical data it becomes apparent that the driving force for an electron transfer from the photogenerated $*[Ru(terpy)_2]^{2+}$ excited state to the diiron portion is uphill by 0.59 eV. We anticipate, however, that protonation of the nitrogen in the ADT bridge in **1** will shift the reduction potential toward more positive values, thereby rendering this process thermodynamically more favorable. Alternatively, introduction of different ligands on the diiron core, followed by protonation of the iron−iron bond, could have a similar effect. Finally, a photogenerated Ru(I) species, which is higher in energy than the Ru(II) excited state, could provide sufficient reducing power to drive an electron transfer to the biomimetic model of the iron hydrogenase. Efforts in these directions are currently in progress.

Experimental Section

A STOE-IPDS image plate diffractometer with a rotating-anode using MoKα radiation ($\lambda = 0.71073$ Å) was used for the single-crystal data collection. Selected crystallographic data for compounds **2**, **4**, and **5** are given in Table 4. The intensities of the reflections were integrated with the STOE software, and the numerical absorption corrections were performed with the programs X-RED and X-SHAPE.[53] The structures were solved by direct methods and refined by full matrix least-squares on F^2 using the SHELX97 and SHELXS97 software, respectively.[54,55]

Cyclic voltammograms were recorded using a Autolab Potentiostat (Ecochimie Netherlands), controlled by GPES software (version 4.8). A glassy carbon disk electrode (diameter 3 mm) was used as the working electrode and was polished prior to each experiment using an aqueous alumina powder slurry. A platinum wire served as a counter and a nonaqueous Ag/Ag^+ was used as reference electrode. All potentials are given vs the $Fc^{+/0}$ couple. The oxidation potentials of the diiron complexes are anodic peak potentials E_{pa}, and the reduction potentials are given as cathodic peak potentials E_{pc}. Cyclic voltammograms were obtained for 1 mM solutions of the analyte in dry acetonitrile, containing 0.1 M tetrabutylammonium hexafluorophosphate as supporting electrolyte at a scan rate of 50 mV/s.

NMR spectra were measured on a Variant 300 MHz machine. All electrospray mass spectra were acquired using a Bruker Daltonics BioAPEX-94e superconducting 9.4 T Fourier transform ion cyclotron resonance (FTICR) mass spectrometer (Bruker Daltonics, Billerica, MA) in broadband mode. A home-built apparatus controlled the direct infusion of sample. The sample was delivered dissolved in 100% ACN using a helium gas container at a pressure of 1.3 bar, pushing the sample through a 30 cm fused silica capillary of inner diameter 20 μm. The flow rate was approximately 100 nL/min. The ion source was coupled to an

(53) X-RED and X-SHAPE, STOE, Crystal Optimisation for Numerical Absorption Corrections; Darmstadt, 1997.
(54) Sheldrick, G. M. *Acta Crystallogr.* **1994**, *A46*, 467.
(55) Sheldrick, G. M. SHELX97. Computer Program for the Refinement of Crystal Structures, Release 97-2; Sheldrick, G. M., Ed.; University of Göttingen: Göttingen, Germany, 1997.

Analytica atmosphere vacuum interface (Analytica of Branford, CT), and a potential difference of 2−4 kV was applied across a distance of approximately 5 mm between the spraying needle and the inlet capillary.

UV/vis absorption spectra were measured on a Varian Cary 50 Bio spectrophotometer. The solvent used in the emission studies was acetonitrile of spectroscopic grade (Merck). The emission spectra were recorded on a SPEX-Fluorolog II fluorimeter. Spectra at 77 K were taken in dry butyronitrile solution in a coldfinger Dewar. The infrared spectra were recorded on Perkin-Elmer Spectrum 1. The time correlated single photon counting setup was pumped with 100 kHZ pulses of 150 fs width generated in a regenerative amplified Ti:Sapphire system from Coherent. The wavelengths used for the experiments was 400 nm obtained from doubling of the fundamental 800 nm light. The sample was contained in a 1 × 1 cm quartz cuvette, and the emission light was collected at magic angle conditions compared to the excitation light. A 400 nm interference filter was used before the sample, and different combinations of interference and cut off filters after the sample were used to remove unwanted wavelengths. Emitted light was collected by a water cooled Hammamatsu R38094-5 MCP-PMT and resulted in a response function with a fwhm of 65 ps. Flash photolysis experiments were performed with a frequency tripled Q-switched Nd:YAG laser from Quantel. The out coming light pumped an OPO generating <10 ns flashes tunable in the range 410−660 nm. Analyzing light was provided by a pulsed 100 W Xe-lamp used in a spectrometer system from Applied Photophysics. Average energy of the laser pulses was 25 mJ.

p-Formaldehyde, 4-iodoaniline, 4-bromoaniline, thionyl chloride, $[Pd(PPh_3)_2Cl_2]$, CuI, and phenyl acetylene were purchased from commercial suppliers and used as obtained. $[(\mu\text{-}S_2)Fe_2(CO)_6]$,[29] 4′-[((trifluoromethyl)sulfonyl)oxy]-2,2′:6′,2″-terpyridine,[34] 4′-ethynyl-2,2′:6′,2″-terpyridine,[35] iodo-4-(*N*-piperidyl)benzene,[39] and [(terpy)-$RuCl_2$(DMSO)] were synthesized according to their respective literature procedure. *N*,*N*-Di(chloromethyl)-4-haloaniline and $(\mu\text{-}SCH_2N(4\text{-halophenyl})CH_2S)[Fe(CO)_3]_2$ were synthesized in analogy to the published procedures.[25] The synthesis and characterization of **1** and **6** have been reported elsewhere.[23]

***N,N*-Bis(chloromethyl)-4-bromoaniline.** *p*-Formaldehyde (780 mg, 25 mmol) was added to a solution of 4-bromoaniline (1.72 g, 10 mmol) in CH_2Cl_2 (12 mL). The resulting slurry was stirred at room temperature for 3 h, before thionyl chloride (2.9 mL, 40 mmol) was added dropwise. After having been stirred for further 30 min, the solvents were removed in vacuo, and the remaining solid was dried at 0 °C at high vacuum. The product was practically pure by NMR analysis and was used without further purification. ^{1}H NMR ($CDCl_3$): 7.46 (d, J = 9.0 Hz, 2 H), 7.09 (d, J = 9.0 Hz, 2 H), 5.48 (s, 4 H, NCH_2Cl).

***N,N*-Bis(chloromethyl)-4-iodoaniline.** This compound was synthesized in analogy to the preparation of *N*,*N*-bis(chloromethyl)-4-bromoaniline, starting from 4-iodoaniline. ^{1}H NMR ($CDCl_3$): 7.64 (d, J = Hz, 2 H), 6.98 (d, J = Hz, 2 H), 5.47 (s, 4 H, NCH_2Cl); ^{13}C NMR ($CDCl_3$): 143.0, 138.4, 118.2, 86.1, 65.4.

$[(\mu\text{-}SCH_2N(4\text{-Bromophenyl})CH_2S)Fe_2(CO)_6]$ (2). Super hydride ($LiBEt_3H$, 1 M solution in THF, 2.06 mL, 2.06 mmol) was added to a degassed solution of $[(\mu\text{-}S_2)Fe_2(CO)_6]$ (344 mg, 1 mmol) in THF (25 mL) at − 78 °C over 10 min. *N*,*N*-Bis(chloromethyl)-4-bromoaniline (540 mg, 2 mmol) was added to the green solution, causing an immediate change in color to red. After the reaction mixture was allowed to warm to room temperature, the solvent was removed in vacuo, and the resulting red solid was purified by column chromatography (silica, 20% toluene in hexane). Red solid, 412 mg (0.76 mmol, 76%). Elemental analysis (%) calcd for $C_{14}H_8BrFe_2NO_6S_2$: C 31.03, H 1.48, N 2.59; found: C 31.21, H 1.62, N 2.56; ^{1}H NMR ($CDCl_3$): 7.39 (d, J = 9.0 Hz, 2 H), 6.61 (d, J = 9.0 Hz, 2 H), 4.26 (s, 4 H, NCH_2S); ^{13}C NMR ($CDCl_3$): 206.9, 143.8, 132.7, 117.4, 112.8, 49.7; IR(CH_2Cl_2): ν_{CO} 2077, 2038, 2000.

$[(\mu\text{-}SCH_2N(4\text{-Iodophenyl})CH_2S)Fe_2(CO)_6]$ (3). This compound was synthesized in analogy to the preparation of **2**, starting from *N*,*N*-bis(chloromethyl)-4-iodoaniline (632 mg, 2 mmol). Red solid, 451 mg (0.76 mmol, 76%). Elemental analysis (%) calcd for $C_{14}H_8Fe_2NO_6S_2I$: C 28.55, H 1.37, N 2.38; found: C 28.66, H 1.43, N 2.24; ^{1}H NMR ($CDCl_3$): 7.40 (d, J = 9.0 Hz, 2 H), 6.63 (d, J = 9.0 Hz, 2 H), 4.29 (s, 4 H, NCH_2S); ^{13}C NMR ($CDCl_3$): 206.8, 144.4, 138.6, 117.9, 82.3, 49.5; IR(CH_2Cl_2): ν_{CO} 2076, 2038, 2000.

$[(\mu\text{-}SCH_2N(4\text{-Bromophenyl})CH_2S)Fe_2(CO)_5(PPh_3)]$ (4). $[(\mu\text{-}SCH_2N(4\text{-bromophenyl})CH_2S)Fe_2(CO)_6]$ (40 mg, 0.075 mmol) was dissolved in degassed *n*-propylamine (10 mL), and triphenylphosphine (65 mg, 0.25 mmol) was added. After 5 h of stirring at reflux, TLC control indicated that all starting material had been consumed. The red residue, obtained after removal of the solvent in vacuo, was subjected to column chromatography (silica, 50% toluene in hexane). Red solid, 43 mg (0.055 mmol, 74%). Elemental analysis (%) calcd for $C_{31}H_{23}BrFe_2NO_5PS_2$: C 47.92, H 2.99, N 1.80; found: C 47.70, H 2.96, N 1.70; ^{1}H NMR ($CDCl_3$): 7.73 (m, 6 H), 7.45 (m, 9 H), 7.27 (d, J = 7.8 Hz, 2 H), 6.43 (d, J = 7.8 Hz, 2 H), 3.98 (d, J = 12.2 Hz, 2 H), 2.95 (d, J = 12.2 Hz, 2 H); ^{13}C NMR ($CDCl_3$): 212.9, 212.7, 208.6, 145.3, 135.7, 135.1, 133.6, 133.5, 132.2, 130.4, 130.3, 128.7, 128.6, 117.1, 111.7, 47.0; IR-(CH_2Cl_2): ν_{CO} 2048, 1990, 1935.

$[\mu\text{-}SCH_2N(4\text{-Trimethylsilylethynylphenyl})CH_2S][Fe(CO)_3]_2$ (5). $[(PPh_3)_2PdCl_2]$ (7 mg, 0.01 mmol) and CuI (2 mg, 0.01 mmol) were added successively to a degassed solution of iodoarene **3** (59 mg, 0.1 mmol) and trimethylsilylacetylene (20 mg, 0.2 mmol) in triethylamine (8 mL) at 40 °C. After 90 min of stirring at this temperature, the mixture was concentrated in vacuo, and the black residue was subjected to column chromatography (silica, 40% toluene in hexanes). The title compound was afforded as a red solid, 51 mg (0.091 mmol, 91%). Single crystals suitable for X-ray analysis were grown from concentrated pentane solutions at −20 °C. Elemental analysis (%) calcd for $C_{19}H_{17}Fe_2NO_6S_2Si$: C 40.81, H 3.06, N 2.50; found: C 40.96, H 3.00, N 2.41; ^{1}H NMR ($CDCl_3$): 7.57 (d, J = 9.0 Hz, 2 H), 6.50 (d, J = 9.0 Hz, 2 H), 4.26 (s, 4 H, NCH_2S); ^{13}C NMR ($CDCl_3$): 206.8, 144.4, 133.8, 115.1, 114.6, 105.0, 93.0, 49.5, 0.1; IR(CH_2Cl_2): $\nu_{C=C}$ 2153, ν_{CO} 2076, 2038, 2001.

4′-(4-*N*-Piperidylphenylethynyl)-2,2′:6′,2″-terpyridine (7a). Copper iodide (2 mg, 0.01 mmol) was added to a degassed solution of 4-*N*-piperidyliodobenzene (38 mg, 0.13 mmol), 4′-ethynyl-2,2′:6′,2″-terpyridine (34 mg, 0.13 mmol) and $[Pd(PPh_3)_2Cl_2]$ (7 mg, 0.01 mmol) in toluene, and Et_3N (1:1, 10 mL) at 70 °C. After having been stirred at this temperature for 3 h, the solvents were removed in vacuo, and the resulting black solid was subjected to column chromatography (silica, 2% acetone in CH_2Cl_2). Tan white solid, 33 mg (0.08 mmol, 61%). ^{1}H NMR ($CDCl_3$): 8.69 (m, 2 H), 8.59 (m, 2 H), 8.51 (s, 2 H), 7.84 (m, 2 H), 7.42 (d, J = 8.7 Hz, 2 H), 7.31 (m, 2 H), 6.86 (d, J = 8.7 Hz, 2 H), 3.24 (m, 4 H), 1.65 (m, 6 H); ^{13}C NMR ($CDCl_3$): 155.9, 155.3, 151.8, 149.1, 136.8, 134.2, 133.2, 123.9, 122.5, 121.2, 115.0, 111.2, 95.3, 86.2, 49.4, 25.4, 24.3.

4′-(Phenylethynyl)-2,2′:6′,2″-terpyridine (7b). This compound was synthesized in a procedure analogous to that for the preparation of ligand **7a**, starting from phenyl acetylene (61 mg, 0.6 mmol) and 4′-[((trifluoromethyl)sulfonyl)oxy]-2,2′:6′,2″-terpyridine (114 mg, 0.3 mmol). White solid, 83 mg (0.25 mmol, 83%). ^{1}H NMR

($CDCl_3$): 8.69 (m, 2 H), 8.58 (m, 2 H), 8.55 (s, 2 H), 7.82 (m, 2 H), 7.56 (m, 2 H, Ph), 7.36 (m, 3 H, Ph), 7.30 (m, 2 H); ^{13}C NMR ($CDCl_3$): 155.6, 155.4, 149.1, 136.8, 133.3, 131.9, 129.0, 128.4, 123.9, 122.8, 122.4, 121.2, 93.7, 87.5.

[(Terpy)Ru(4′-(4-*N*-Piperidylphenylethynyl)-2:2′,6′:2″-terpyridine)] (PF_6)$_2$ (8a). [(Terpy)$RuCl_2$·DMSO] (20 mg, 0.04 mmol) was added to a degassed solution of ligand **7a** (17 mg, 0.04 mmol) in ethanol (20 mL). After stirring at reflux for 16 h, the solvent was removed in vacuo, and the resulting red solid was subjected to flash chromatography (silica, CH_3CN:H_2O:saturated aqueous KNO_3 = 90:9:1). The fractions containing product were concentrated in vacuo, and the remaining red solid was dissolved in water (5 mL) to which a saturated aqueous solution of NH_4PF_6 (10 mL) was added. After extraction with CH_2Cl_2) (3*15 mL) the combined organic layers were washed with a saturated aqueous solution of NH_4PF_6 (2*15 mL) and dried over Na_2SO_4. Filtration and removal of the solvent in vacuo was followed by recrystallization from CH_2Cl_2/Et_2O to afford the title compound as a red solid, 22 mg (0.021 mmol, 53%). Elemental analysis (%) calcd for $C_{43}H_{35}F_{12}N_7P_2Ru$: C 49.59, H 3.39, N 9.41; found: C 49.41, H 3.62, N 9.24; ^{1}H NMR (CD_3CN): 8.78 (s, 2 H), 8.73 (d, J = 8.4 Hz, 2 H), 8.47 (m, 4 H), 8.40 (t, J = 8.4 Hz, 1 H), 7.91 (m, 4 H), 7.59 (d, J = 9.0 Hz, 2 H), 7.39 (m, 2 H), 7.32 (m, 2 H), 7.15 (m, 4 H), 7.03 (d, J = 9.0 Hz, 2 H), 3.37 (m, 4 H), 1.67 (m, 6 H); ^{13}C NMR (CD_3CN): 158.9, 158.7, 156.2, 156.1, 153.6, 153.5, 139.1 (2 H), 136.9, 134.5, 132.1, 128.5, 128.4, 125.6, 125.4 (2 H), 124.7, 115.6, 109.6, 100.4, 86.3, 49.4, 26.2, 25.1; FTICR ESI-MS: Ru-isotopic pattern centered at m/z = 896.19 (100%) [M − PF_6^-]$^+$, calcd for [M − PF_6^-]$^+$: m/z = 896.16.

[(Terpy)Ru(4′-(Phenylethynyl)-2:2′,6′:2″-terpyridine)] (PF_6)$_2$ (8b). Synthesized in analogy to **8a**, starting from ligand **7b** (77 mg, 0.23 mmol) and [(terpy)$RuCl_2$·DMSO] (111 mg, 0.23 mmol). Red solid, 141 mg (0.15 mmol, 64%). Elemental analysis (%) calcd for $C_{38}H_{26}F_{12}N_6P_2Ru$: C 47.66, H 2.74, N 8.77; found: C 47.42, H 2.90, N 8.72; ^{1}H NMR (CD_3CN): 8.90 (s, 2 H), 8.78 (d, J = 8.1 Hz, 2 H), 8.53 (m, 4 H), 8.42 (t, J = 8.1 Hz, 1 H), 7.92 (m, 4 H), 7.79 (m, 2 H, Ph), 7.56 (m, 3 H, Ph), 7.38 (m, 4 H), 7.17 (m, 4 H); ^{13}C NMR (CD_3CN): 158.9, 158.6, 156.4, 156.2, 153.6, 153.5, 139.2 (2 H), 137.1, 133.1, 131.3, 131.0, 130.1, 128.7, 128.5, 126.2, 125.6, 125.5, 124.8, 122.3, 97.7, 87.2; FTICR ESI-MS: Ru-isotopic pattern centered at m/z = 813.11 (100%) [M − PF_6^-]$^+$, calcd for [M − PF_6^-]$^+$: m/z = 813.09.

Acknowledgment. Financial support for this work was provided by the Swedish Energy Agency, the Knut and Alice Wallenberg Foundation, and the Swedish Research Council (VR). J. B. acknowledges the financial support by grants from the Knut and Alice Wallenberg Foundation and the Swedish Research Council (621-2002-5261, 629-2002-6821). L.H. acknowledges a research fellow position from the Royal Swedish Academy of Science.

Supporting Information Available: A cyclic voltammogram typical for [(μ-ADT)$Fe_2(CO)_6$] type complexes and emission decay traces for complexes **1** and **8b**. This material is available free of charge via the Internet at http://pubs.acs.org.

IC0303385